

# Assessment of Stray Grain Formation in Weld Joint of Single Crystal Molybdenum by ANSYS FE Simulation

Ma Yan, Xu Yanze, Wang Jianju

North China Electric Power University, Beijing 102206, China

**Abstract:** Stray grains were observed in an electron beam welded (EBW) joint of single crystal molybdenum (Mo) in former studies. In the present paper, finite element (FE) method, combining the theoretical analysis, was used for evaluating the stray grain formation. Temperature-dependent thermal properties of molybdenum were incorporated in the model and a 3D volumetric moving double-ellipsoid heat source was applied. The relationship of parameter  $\Phi$ , describing the degree of stray grain formation, to the thermal gradient  $G$  and the growth velocity  $V$  was used. Temperature and thermal gradient data of the model were extracted from simulation results under different operating conditions, and  $\Phi$  was calculated. The effects of the welding parameters, including welding power  $Q$  and welding speed  $S$  on the formation of the weld stray grain were obtained.

**Key words:** stray grains; single crystal molybdenum; EBW; ANSYS

Due to its good creep properties, single crystal molybdenum is widely used as high-temperature resistant components in the aerospace field<sup>[1,2]</sup>. Electron Beam Welding (EBW), which is of high energy density and deep weld penetration, is used for joining single crystal Mo. However, to obtain desirable single crystal weld joint is still a big challenge<sup>[3,4]</sup>. The primary reason is that during weld solidification constitutional supercooling just ahead of the solidification can lead to the formation of stray grains; if this extends enough, the single crystal solidification microstructure will be replaced by a polycrystalline microstructure, leading to a decrease of mechanical properties<sup>[5,6]</sup>. Therefore, it is greatly significant to investigate the effect of the welding parameters on the formation of the weld stray grain.

In this study, we used FE method to compute the temperature and thermal gradient field through the software ANSYS with a dynamic 3D double ellipsoid welding heat source. The effects of the welding parameters on the formation of the weld stray grain were discussed.

## 1 Simulation Model Description

### 1.1 Heat source model

Single crystal Mo tube with 20 mm in external diameter and 4 mm in thickness was welded by orientation EBW. Different models of heat loading was used to inspect the behavior of temperature gradient at different depths. These heat models include double ellipsoid heat source model and Gauss heat source model. Simulated results in ANSYS show that Gauss heat source temperature field distribution is not uniform and cannot be used to describe the shape of microstructure of the electron beam welding accurately. And the distribution of the temperature field in the double ellipsoid heat source model is similar to that of the molybdenum alloy. So ANSYS with a dynamic 3D double ellipsoid welding heat source presented by Goldak et al<sup>[7,8]</sup> was used to simulate this EBW processes. The double-ellipsoidal heat source model, as shown in Fig.1, can simulate and analyze the thermal fields of deep penetration weld.

In this model, the double-ellipsoidal heat source,  $q(x, y, z)$  describing the heat flux distributions inside heat source and the power density distribution inside the front quadrant can be expressed as:

Received date: September 12, 2017

Foundation item: Beijing Natural Science Foundation (2162040)

Corresponding author: Ma Yan, Ph. D., Associate Professor, School of Nuclear Science and Engineering, North China Electric Power University, Beijing 102206, P. R. China, Tel: 0086-10-61773161, E-mail: mayan@ncepu.edu.cn

Copyright © 2018, Northwest Institute for Nonferrous Metal Research. Published by Elsevier BV. All rights reserved.

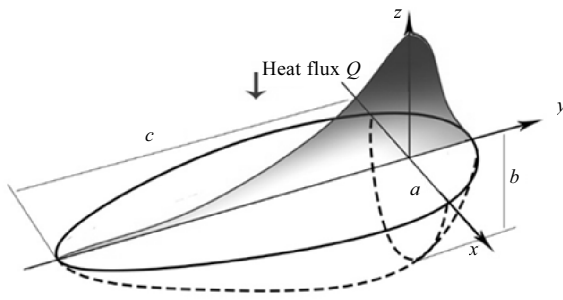


Fig. 1 Double ellipsoid heat source configuration

$$q(x, y, z) = \frac{6\sqrt{3}f_f Q}{abc\pi\sqrt{\pi}} e^{-3x^2/a^2} e^{-3y^2/b^2} e^{-3z^2/c^2} \quad (1)$$

The power density distribution inside the rear quadrant can be expressed as:

$$q(x, y, z) = \frac{6\sqrt{3}f_r Q}{abc\pi\sqrt{\pi}} e^{-3x^2/a^2} e^{-3y^2/b^2} e^{-3z^2/c^2} \quad (2)$$

where  $Q$  is the energy input rate,  $f_f$  and  $f_r$  are fractional factors of the heat deposited in the front and rear quadrant, respectively, and  $f_f + f_r = 2$ ;  $a$ ,  $b$ , and  $c$  are the heat source parameters. Heat source parameters are given in Table 1.

### 1.2 Finite element model

EBW numerical model was built using finite element analysis software ANSYS 14.5. At the stage of thermal analysis, the effect of mechanical deformation on heat flow has been ignored.

The given structure as shown in Fig.2, a short tube with 4 mm wall thickness and 20 mm in external diameter, was modeled using thermal element SOLID70 which has a 3D transient thermal analysis capability

The thermal properties used in this work are temperature dependent as given in Table 2.

Data shown in Table 2 are obtained by curve fitting from raw data. The melting point is 2624 °C. Situations of thermal conductivity above the melting point are complicated. Heat transfer enhancement caused by liquid exchange at weld pool and heat transfer deterioration caused by phase transition become difficult to untangle. So thermal conductivity used in the liquid state is a hypothetical value. The fixed cross section of weld pool along its flow path was chosen for research, and this cross section of weld pool helped to examine the process of melting and solidification. Using ANSYS simulation, the solidification process of weld pool can be seen clearly. Data for temperature distribution across the pool and its gradient were obtained at different depths of 0.45h, 0.63h, 0.77h, 0.89h, and 1.00h to calculate  $\Phi$  for selected points. The “h” indicates the maximum depth of weld pool.

Table 1 Heat source parameters used in this work

Parameter	Value
Welding heat source half width, $a$ /mm	1
Welding heat source depth, $b$ /mm	3
Heat source distance of front quadrant, $c_1$ /mm	1
Heat source distance of rear quadrant, $c_2$ /mm	2
Fraction of heat deposited in front quadrant, $f_f$	0.6
Fraction of heat deposited in rear quadrant, $f_r$	1.4
Welding thermal efficiency	0.95

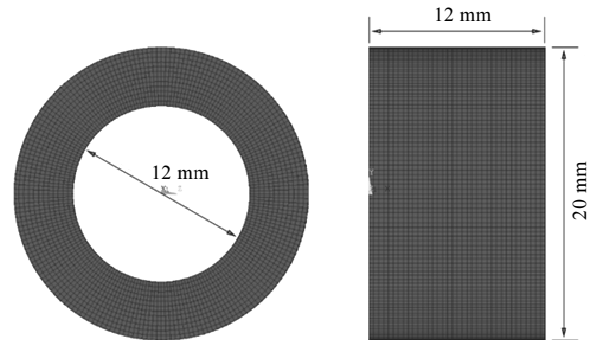


Fig. 2 3D model tube ring

Table 2 High-temperature thermodynamic properties of Mo<sup>[9]</sup>

$T/^\circ\text{C}$	$\lambda/\times 10^2$ $\text{W}\cdot(\text{m}\cdot^\circ\text{C})^{-1}$	$H/\times 10^9$ $\text{J}\cdot\text{m}^{-3}$	$C/\times 10^2$ $\text{J}\cdot(\text{kg}\cdot^\circ\text{C})^{-1}$
25	1.38	0.00	2.53
200	1.31	0.463	2.65
500	1.19	1.31	2.84
750	1.11	2.06	2.99
1000	1.03	2.83	3.15
1500	0.932	4.53	3.53
2000	0.876	6.50	4.17
2500	0.841	8.88	5.29
2618	0.837	9.54	5.74
2630	1.11	12.5	4.21
3000	1.11	14.0	4.21
4000	1.11	17.9	4.21

Note:  $\lambda$ -thermal conductivity,  $H$ -enthalpy,  $C$ -heat capacity

## 2 Numerical Analysis Procedure

### 2.1 Calculation of areal fraction of stray grains ( $\Phi$ )

Stray grain formation is the result of constitutional supercooling, which is controlled by the temperature gradient in the liquid directly ahead of the solid/liquid interface and the growth rate<sup>[10]</sup>. The conditions for nucleation and growth of equiaxed grains in front of the advancing solidification front lead to stray grain formation. Parameter  $\Phi$  is defined as the areal fraction ahead of the advancing solidification front that is composed of newly nucleated grains. Parameter  $\Phi$  is evaluated quantitatively by Hunt<sup>[11]</sup> and Gaumann et al<sup>[12,13]</sup>. The equation used to calculate  $\Phi$  is given by:

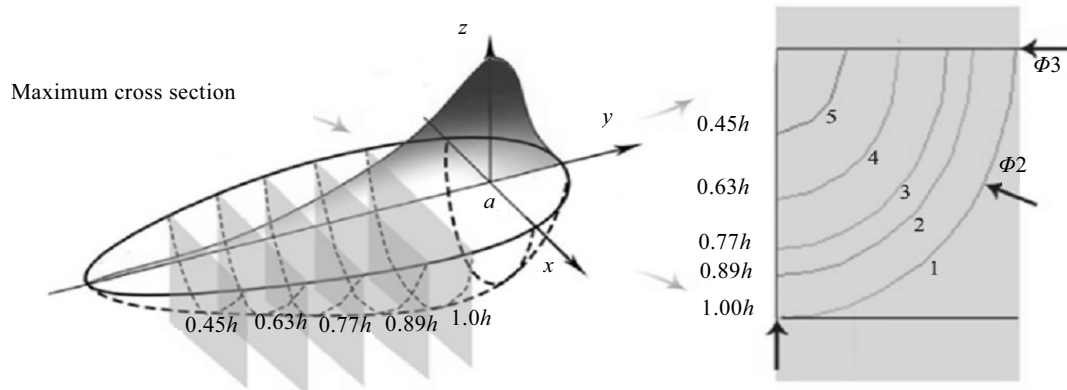


Fig.3 Schematic diagram of data collecting location

Table 3 Φ of all the data collecting locations

No.	Section number	Φ <sub>1</sub>	Φ <sub>2</sub>	Φ <sub>3</sub>	Φ <sub>ave</sub>
1	11	0.351	0.066	0.088	0.168
	12	0.940	0.728	0.734	0.801
	13	0.987	0.986	0.899	0.957
	14	0.994	0.990	0.984	0.989
	15	0.999	0.997	0.998	0.998
2	21	0.236	0.086	0.083	0.135
	22	0.517	0.539	0.371	0.475
	23	0.593	0.559	0.572	0.575
	24	0.771	0.720	0.672	0.721
	25	0.812	0.772	0.799	0.794
3	31	0.130	0.027	0.019	0.059
	32	0.262	0.097	0.133	0.164
	33	0.271	0.189	0.142	0.201
	34	0.243	0.173	0.215	0.210
	35	0.263	0.226	0.244	0.244
4	41	0.115	0.044	0.025	0.061
	42	0.384	0.244	0.211	0.280
	43	0.308	0.409	0.411	0.376
	44	0.450	0.375	0.471	0.432
	45	0.514	0.533	0.496	0.514
5	51	0.112	0.001	0.005	0.039
	52	0.781	0.746	0.538	0.688
	53	0.956	0.778	0.771	0.835
	54	0.973	0.972	0.958	0.968
	55	0.992	0.989	0.981	0.988
6	61	0.179	0.022	0.026	0.076
	62	0.181	0.061	0.064	0.102
	63	0.197	0.099	0.099	0.132
	64	0.213	0.112	0.152	0.159
	65	0.221	0.221	0.221	0.221

$$\Phi = 1 - \exp\left(-\frac{4\pi N_0}{3} \left(\frac{1}{(n+1)(G^n/aV)^{1/n}}\right)^3\right) \quad (3)$$

Where *a* and *n* are material constants and *N*<sub>0</sub> is the nuclei density. Temperature *T* and thermal gradient *G* of the model at any time can be extracted from simulation results. The

data clearly represents weld pools under different operating conditions. And the growth velocity *V* can be calculated with thermal gradient *G* and welding speed *S*.

### 2.2 Option of data collecting location

Parameter Φ is decided by the rear part, which is behind the maximum cross section of the weld pool. Cross sections perpendicular to the direction of welding are used to split the rear part. Fig.3 shows a schematic diagram of the intersected weld pool.

In every section, three data collecting locations are selected. The average of fifteen pieces of data drawn from five sections is the Φ for one weld joint.

## 3 Results and Discussions

The calculated Φ is listed in Table 3 and Table 4. Φ in Table 4 is the average values of fifteen pieces of data in Table 3 drawn from five sections under six different welding conditions.

### 3.1 Effect of welding power

The value of Φ is plotted as a function of welding power at 4 mm/s welding speed, as shown in Fig.4. It can be seen that parameter Φ of the whole weld and centerline increase with increasing welding power. It means that more stray grains are generated with the increase in welding heat input.

Table 4 Calculated Φ as a function of weld condition

No.	Q/W	S/mm·s <sup>-1</sup>	Φ
1	1200	2	0.783
2	1200	3	0.540
3	1200	4	0.176
4	1400	4	0.333
5	1600	4	0.704
6	1200	5	0.138

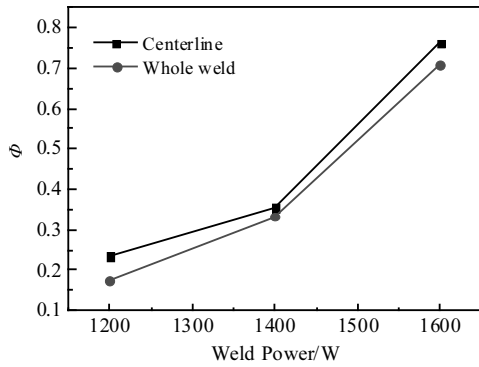


Fig.4 Plot of  $\Phi$  versus welding power at 4 mm/s

**3.2 Effect of welding speed**

The value of  $\Phi$  is plotted as a function of welding speed at 1200 W welding power, as shown in Fig.5. It can be seen that parameter  $\Phi$  of the whole welding and centerline decrease by increasing the welding speed  $S$ . It means that more stray grains are generated with the decrease in welding speed.

**3.3 Comparison of results with metallograph**

Metallographs of the cross section of weld of single crystal Mo tube are shown in Fig.6. It shows that stray grains are mainly found near the weld centerline, especially

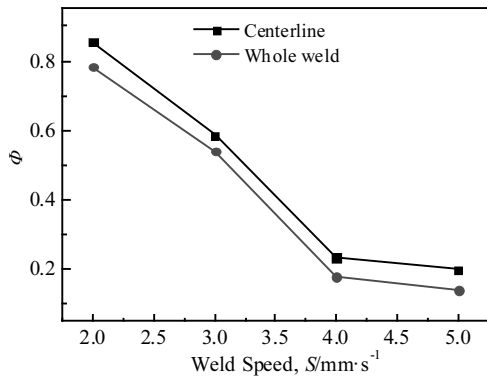


Fig.5 Plot of  $\Phi$  versus welding speed  $S$  at 1200 W

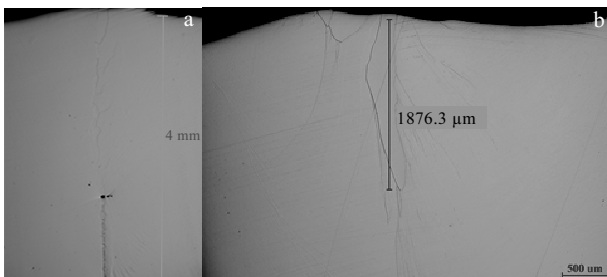


Fig.6 Metallographs of cross section of EBW joint: (a) the whole joint (lack of penetration at the half bottom) and (b) the top of the weld joint

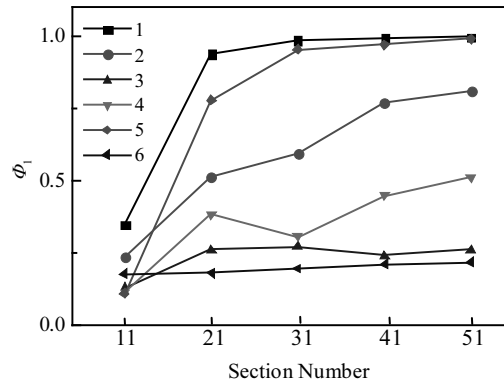


Fig.7 Parameter  $\Phi$  at the three locations under different conditions (1~6)

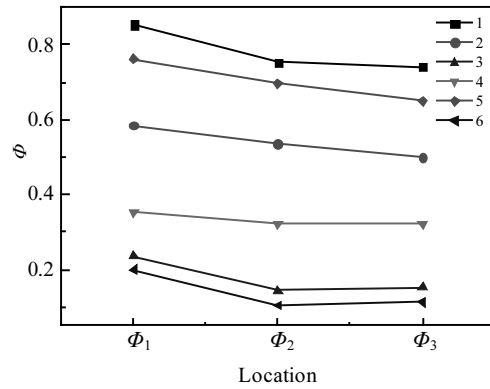


Fig.8 Parameter  $\Phi$  at the centerlines under different conditions (1~6)

at the top of centerline (near red line). This accords with the simulation result, as shown in Fig.7 and Fig.8. Parameter  $\Phi$  of stray grains at centerline, especially at the top of centerline, tend to be larger.

**4 Conclusions**

1) The simulation results and experimental results of a specific welding procedure display parameter  $\Phi$  of stray grains tend to be larger near the weld centerline, especially the top of center line. This means that the driving force of stray grains near the centerline, especially at the top of center line, is greater.

2) Numerical simulation results show that parameter  $\Phi$  of the whole weld and the weld centerline increases with the welding heat input increasing, at 4 mm/s welding speed.

3) At 1200 W welding power, parameter  $\Phi$  of the whole welding and centerline decrease by increasing the welding speed.

**Acknowledgement:** Authors acknowledge China Institute of Atomic Energy for the experimental help.

## References

- 1 Hu Z W, Li Z K, Zhang Q et al. *Rare Metal Materials and Engineering*[J], 2007, 36(12): 2254 (in Chinese)
- 2 Hu Z W, Li Z K, Yin T et al. *Rare Metal Materials and Engineering*[J], 2010, 34(1): 48 (in Chinese)
- 3 Li X, Jiang W, Chen S J. *Rare Metal Materials and Engineering*[J], 2015, 44(1): 189 (in Chinese)
- 4 Jiang W, Zheng J P, Li X et al. *Welding & Joining*[J], 2016, 7: 37 (in Chinese)
- 5 Vitek J M. *Acta Materialia*[J], 2005, 53(1): 53
- 6 Vitek J M, Babu S S, Park J W et al. *Proc Superalloys*[C]. Warrendale: TMS, 2004: 459
- 7 Goldak J, Chakravarti A, Bibby M. *Metallurgical Transactions B*[J], 1984, 15(2): 299
- 8 Mo C L, Yu S F, Qian B N et al. *Transactions of the China Welding Institution*[J], 2001, 22(3): 93 (in Chinese)
- 9 Desai P D. *Journal of Physical and Chemical Reference Data*[J], 1987, 16(1): 91
- 10 Park J W, Vitek J M, Babu S S et al. *Science and Technology of Welding & Joining*[J], 2004, 9(6): 472
- 11 Hunt J D. *Materials Science and Engineering*[J], 1984, 65(1): 75
- 12 Gäumann M, Bezencon C, Canalis P et al. *Acta Materialia*[J], 2001, 49(6): 1051
- 13 Gäumann M, Trivedi R, Kurz W. *Materials Science and Engineering A*[J], 1997, 226: 763

## 基于 ANSYS 模拟评估 Mo 单晶电子束焊接焊缝中的离散晶粒

马 雁, 许雁泽, 王剑举

(华北电力大学, 北京 102206)

**摘 要:** 以往的研究中发现在钼单晶电子束焊接焊缝中形成了离散晶粒。本研究基于有限元模拟对杂散晶粒在钼单晶焊缝中的产生行为进行了分析。利用 ANSYS 软件, 采用双椭球 3D 移动热源, 对钼单晶圆管的电子束焊接接头进行有限元数值模拟。使用了用以描述晶粒离散程度的参数  $\phi$  和熔池凝固前方温度梯度  $G$ 、晶体生长速度  $V$  关系的模型。通过不同焊接工艺下的模拟结果提取温度和温度梯度数据, 获得  $G$  和  $V$ , 计算得  $\phi$ , 获得焊接功率和焊接速度对钼单晶焊缝中杂散晶粒形成的影响。

**关键词:** 离散晶粒; 钼单晶; 电子束焊接; ANSYS

---

作者简介: 马 雁, 女, 1973 年生, 博士, 副教授, 华北电力大学核科学与工程学院, 北京 102206, 电话: 010-61773161, E-mail: mayan@ncepu.edu.cn